J. Fluid Mech. (1971), *vol.* 45 *part* 1, *pp.* 189–201
Printed in Great Britain

Viscous flow in a deformable rotating container

By STEVEN T. SUESS

ESSA Research Laboratories,
Boulder, Colorado 80302

(Received 9 February 1970 and in revised form 28 August 1970)

The steady-state flow in a rotating container is examined when the container is deformed into an ellipsoidal figure which is fixed in inertial space. The analysis is carried out for a fluid of small viscosity, and to the second order in Rossby number. Results show a vortex existing along the rotation axis, this being an interior manifestation of non-linear boundary-layer effects. These effects are a direct consequence of the forced oscillation being at twice the rotational frequency. The configuration is chosen to suggest the effects of gravitational body tides on the dynamics of the core of the earth. This problem is related to the similar problem of a precessing spheroid, and an experiment is described which tests the present theory and confirms previous experimental data from precessing spheroids.

1. Introduction

This paper examines the stationary flow of a slightly viscous and incompressible fluid in a rotating container when the container is deformed into an ellipsoidal figure fixed in inertial space. The objective is to determine the effects caused by the non-axisymmetric shape of the container to second order in Rossby number. There is generally a slight mismatch between the velocity of the interior geostrophic flow and the velocity of the container surface. This results in a forced oscillation in the boundary layer, and a consequent second-order deviation from constant vorticity in the interior. This deviation appears as a line vortex oriented along the vorticity vector of the fluid.

A laboratory experiment is described, which duplicates this model. The results confirm the main aspects of the theory, yet show significant higher-order deviations from the theory. The nature of the dynamic resolution of the singular properties associated with a vortex is discussed, although the details involved in the boundary-layer interaction were not directly observable.

The study of this model is a consequence of an interest in the flow in the core of the earth, the ellipsoidal shape of the container being used to synthesize the effects of gravitational body tides. Such tides could also have an effect on the dynamics of the core of the sun, and may be relevant to other astrophysical problems. The flows are also interesting in their own right because of their physical nature and their mathematical properties.

For this study, the configuration is an ellipsoidal figure, Σ, which rotates about one of its axes and has its figure fixed in an inertial frame of reference. The

velocity, **V**, of the bending or stretching surface, is known. Contained within Σ is an incompressible, Newtonian fluid of kinematic viscosity ν and density ρ. The mean angular velocity of Σ is $\boldsymbol{\omega}$, and the equation for Σ is simply:

$$\Sigma: \frac{x^2}{a^2}+\frac{y^2}{b^2}+\frac{z^2}{c^2} = 1 \tag{1}$$

in a central, non-rotating co-ordinate system aligned along the principle axes of Σ. It will be assumed that

$$\boldsymbol{\omega} = \omega\hat{k}. \tag{2}$$

Since this model is limited to the case in which $\boldsymbol{\omega}$ is aligned along one of the axes of Σ, no tiltover of the vorticity vector away from $\boldsymbol{\omega}$ results. This case is chosen in order to illustrate the new aspects of the biharmonic forcing of the tides, while avoiding an unnecessarily complicated analysis. The non-equatorial deformation produces a tiltover, the direct result of which is analyzed by Busse (1968*a*). In his paper he discusses precession-forced tiltover, but the consequences are the same. A general calculation of the tiltover for an earth model, including gravitational body tides, is given by Suess (1970).

The basic difference between the tiltover and the tidally induced flows is the forcing frequency. For equatorial tides, this frequency is 2ω: for the tiltover, it is ω. Both frequencies correspond to the frequency of an inertial mode of oscillation of the fluid. It should be mentioned that the 2ω inertial mode has been thought to be physically forbidden, because of the singular nature of its predicted velocity and pressure fields. In this paper the theoretical and experimental results confirm the existence of the mode, and the experiment shows the physical resolution of its supposed singular nature. Described with respect to the rotational equator of the fluid, tiltover causes a cylindrical shear zone to occur between the $\pm 30°$ latitude circles. The tides cause a shear zone to occur between the $\pm 90°$ latitude points, or along the axis of rotation of the fluid. This tidal shear is also excited to a lesser degree by the tiltover in a rigid spheroidal container, because the streamlines become slightly elliptical to produce a small 2ω effect. In fact, both experimentally and theoretically, it is only possible to isolate the 2ω effect, the ω effect always produces a higher-order 2ω effect either through the above-mentioned induced ellipticity of the streamlines or through a harmonic excitation.

2. Analysis for an equatorial tide

A stationary solution is sought to the equations of motion, as written in the co-ordinate system used to define Σ in (1). The equations of motion

$$(\mathbf{v}.\nabla)\mathbf{v} = -\nabla(P/\rho)+\nu\nabla^2\mathbf{v}, \tag{3}$$

continuity

$$\nabla.\mathbf{v} = 0, \tag{4}$$

and the viscous fluid boundary condition

$$\mathbf{v} = \mathbf{V} \quad \text{on} \quad \Sigma \tag{5}$$

completely specify the problem. However, even though the problem is well posed, it is not possible to find a general solution which satisfies (5). In order to

find a useful solution, boundary-layer approximations are used, which require that the dissipative terms be small with respect to the pressure gradient and inertial terms—except near Σ. The general procedures used in such an analysis are detailed by Greenspan (1965, 1968), Busse (1968*a*), and Stewartson & Roberts (1963).

The calculation depends on two dimensionless parameters, which in this case are required to be small compared to one. First, there is the Ekman number:

$$E \equiv \nu/\omega a^2. \tag{6}$$

The other parameter is ϵ, the Rossby number. Normally, ϵ is the amplitude of the boundary-layer correction velocity, so that its exact value is a consequence of the model. In proceeding with the analysis, it would quickly be found that a first-order linear solution to (3) and (5) would necessitate an order $E^{\frac{1}{2}}$ correction to satisfy the continuity equation. There would also be a non-linear correction of order ϵ contributed by the advective terms in (3). Instead of making such corrections step by step, it is assumed *a priori* that the variables can be expanded in a double series in powers of $E^{\frac{1}{2}}$ and ϵ. The validity of such an expansion is questionable for powers of E larger than $E^{\frac{1}{2}}$, but in most physical cases the value of E is so small that it is unnecessary to consider higher orders. In addition, experiments confirm the general validity of the theory, and the calculations are asymptotically correct. The formal expansions are written in (7).

$$\mathbf{v} = \mathbf{v}_0^0 + \sum_{\substack{n=1 \\ m=0}}^{\infty\ \infty} E^{\frac{1}{2}m} \epsilon^n \mathbf{v}_m^n, \tag{7a}$$

$$(P/\rho) = (P/\rho)_0^0 + \sum_{\substack{n=1 \\ m=0}}^{\infty\ \infty} E^{\frac{1}{2}m} \epsilon^n (P/\rho)_m^n. \tag{7b}$$

The solution will be carried to order $\epsilon^2 E^0$. Usually the $E^{\frac{1}{2}}$ term would be investigated first, because this resolves some unusual aspects of the mathematics. Here, the first non-linear correction to the flow is of greatest interest physically and experimentally, because the axial shear zone appears first in the $\epsilon^2 E^0$ terms.

Using the characteristic parameters of the model, the variables are non-dimensionalized as follows:

$$t = [\omega^{-1}]t', \quad r = [a]r'. \tag{8a,b}$$

Dimensionless velocities and pressure are found using these scales. Dropping the primes, (3) becomes

$$(\mathbf{v}.\nabla)\mathbf{v} = -\nabla P + E\nabla^2\mathbf{v}; \tag{9}$$

(4) and (5) are unchanged. Supposing there are no significant shears in the interior flow, the following separation is made

$$\mathbf{v} = \mathbf{q} + \mathbf{u}, \quad P = p + \phi, \tag{10a,b}$$

where $\mathbf{q}$ and p are the velocity and pressure in the essentially inviscid interior, and $\mathbf{u}$ and ϕ are the velocity and pressure in the boundary layer. $\mathbf{u}$ accounts for the non-uniqueness of $\mathbf{q}$, as well as completing the satisfaction of the no-slip

boundary condition. The rest of the boundary-layer approximation is contained in the introduction of a scaled boundary-layer co-ordinate

$$\zeta = -(\mathbf{r}-\mathbf{r}_\Sigma).\hat{n}E^{\frac{1}{2}}. \tag{11}$$

$\mathbf{r}_\Sigma$ is the vector to Σ, and $\hat{n}$ is the unit outward normal on Σ. It is assumed that $\mathbf{u}$ is non-zero only near Σ, and separate equations for $\mathbf{q}$ and $\mathbf{u}$ are found. The dissipative terms are now not present in the interior equations, but are of order one in the boundary-layer equations. The expansions (7*a*) and (7*b*) are applied to $\mathbf{q}, \mathbf{u}, p$, and ϕ. $\mathbf{u}$ will have no $\mathbf{u}_0^0$ contribution, since ϵ is defined to be its amplitude. Substituting the expansions into the separated equations results in an infinite set of ordered equations, with the lower orders being of practical interest and theoretical validity. The first consequence, from the boundary-layer continuity equation, is

$$\frac{\partial}{\partial\zeta}(\mathbf{u}_0^1.\hat{n}) = \frac{\partial}{\partial\zeta}(\mathbf{u}_0^2.\hat{n}) = 0. \tag{12}$$

From the boundary conditions, this implies

$$\mathbf{u}_0^1.\hat{n} = \mathbf{u}_0^2.\hat{n} = 0. \tag{13}$$

To keep the expansions consistent as the ellipsoid approaches a sphere, $\mathbf{q}_0^0$ is defined by

$$\mathbf{q}_0^0 = \hat{k}\times\mathbf{r}. \tag{14}$$

Then, the interior order ϵE^0 problem is

$$(\mathbf{q}_0^0.\nabla)\mathbf{q}_0^1 + (\mathbf{q}_0^1.\nabla)\mathbf{q}_0^0 = -\nabla p_0^1, \tag{15}$$

$$\nabla.\mathbf{q}_0^1 = 0, \tag{16}$$

$$(\mathbf{q}_0^0+\epsilon\mathbf{q}_0^1).\hat{n} = 0 \quad \text{on} \quad \Sigma. \tag{17}$$

This is solved exactly by a constant vorticity flow. The only parameter is the equatorial ellipticity which, from (1), is

$$e \equiv \frac{b^2-a^2}{b^2+a^2}. \tag{18}$$

The solution is given by

$$\mathbf{q}_0^0+\epsilon\mathbf{q}_0^1 = \hat{k}\times\mathbf{r}+e(\hat{\imath}y+\hat{\jmath}x). \tag{19}$$

The normally undetermined magnitude of the vorticity has been set equal to 2 (or 2ω in dimensional units), in anticipation that it is the correct value. It is noted that (19) is an exact non-linear solution to (9) and to the continuity equation, failing only by not satisfying the complete boundary condition. It is called a Poincaré type solution (Lamb 1932, p. 724), and is generally valid for tidally deformed precessing and rotating containers when the containers can be described by a second-order figure. This solution is also an exact geostrophic flow, because the container has closed concentric contours, each of constant total height.

Now, the order ϵE^0 boundary-layer equations must be considered. The pressure is removed by performing the operation:

$$\hat{n}\times(\text{equation}) - i\hat{n}\times(\hat{n}\times(\text{equation}))$$

to obtain

$$\left(\frac{\partial^2}{\partial\zeta^2}-2i\hat{k}.\hat{n}\right)(\hat{n}\times\mathbf{u}_0^1+i\mathbf{u}_0^1)=((\hat{n}\times)-i\hat{n}\times(\hat{n}\times))((\hat{k}\times\mathbf{r}.\nabla)\mathbf{u}_0^1-\hat{k}\times\mathbf{u}_0^1), \quad (20)$$

with

$$\epsilon\mathbf{u}_0^1=\mathbf{V}-q_0^0-\epsilon\mathbf{q}_0^1 \quad \text{on} \quad \Sigma. \quad (21)$$

The solution depends upon the explicit form of **V**. If it is taken that, to order e, Σ bends but does not stretch, then the resulting expression for **V** is

$$\mathbf{V}=(1+\tfrac{1}{2}e\cos 2\varphi)\hat{k}\times\mathbf{r}-e\sin 2\varphi\hat{k}\times(\hat{k}\times\mathbf{r}), \quad (22)$$

φ being the azimuthal angle measured from the x axis. Using this, (20) and (21) can be solved exactly. However, consistent with the ordering, the boundary condition shall be applied only to order ϵ, and higher-order terms are then put into the ϵ^2E^0 boundary-layer equation. A solution to (20) is sought which satisfies (20) and (13), and which is zero far from Σ. It is

$$\mathbf{u}_0^1=\frac{e}{4\epsilon}\{[\hat{k}\times\mathbf{r}-i\hat{n}\times(\hat{k}\times\mathbf{r})][e^{2i\varphi}e^{-\lambda_+\zeta}+e^{-2i\varphi}e^{-\lambda_-\zeta}]$$
$$+[\hat{k}\times\mathbf{r}+i\hat{n}\times(\hat{k}\times\mathbf{r})][e^{-2i\varphi}e^{-\lambda_+^*\zeta}+e^{2i\varphi}e^{-\lambda_-^*\zeta}]\}. \quad (23)$$

The quantities with asterisks are complex conjugates, and:

$$\lambda_\pm=(1\pm i)(1\pm\cos\theta)^{\frac{1}{2}}. \quad (24)$$

In keeping with the comments preceding (23),

$$\mathbf{u}_0^1.\hat{n}=0+O(\epsilon),$$
$$\hat{n}=\hat{r}\sin\theta+\hat{k}\cos\theta+O(\epsilon),$$

and so (23) does not exactly satisfy (13). In (24), θ is the colatitude. The roots of λ are to be chosen such that $\mathbf{u}_0^1$ decreases away from Σ. Since $|\mathbf{u}_0^1|=O(1)$, the appropriate value of ϵ can now be taken as

$$\epsilon=e=\frac{b^2-a^2}{b^2+a^2}. \quad (25)$$

The characteristic boundary-layer thickness is

$$\delta_\pm=1/\lambda_\pm, \quad (26)$$

so that a zero in λ indicates the locations where δ becomes infinite. Such zeros are at $\theta=0$, π, the two poles of rotation of the fluid. These singularities imply a breakdown in the boundary-layer theory to this order, the resolution of which requires investigation to higher orders of E. However, the primary physical consequences of the singularities on the bulk of the flow are shown by the next order in ϵ.

It is possible to make two additional observations. First, the higher harmonics, $\sin 2n\varphi$ and $\cos 2n\varphi$, may be present in **V** without seriously modifying $\mathbf{u}_0^1$. This is because the result for $\lambda_\pm^{(n)}$ is

$$\lambda_\pm^{(n)}=(1\pm i)(n\pm\cos\theta)^{\frac{1}{2}}, \quad (27)$$

which has no new zeros, thus resulting in no new singularities. This point is made to show that deviations of **V** from the particular form given by (22) are

insignificant both for radial terms and for higher harmonics. Consequently, the experimental investigation is made simpler since only the amplitude of e and the 2φ general dependence of $\mathbf{V}$ are critical in the results. The other observation is that, by integrating the ϵE^0 continuity equation, it is found that the mass efflux from the boundary in this order is infinite at the points where the boundary-layer thickness becomes infinite.

Before continuing, it will be helpful to review what has been done and to make a few comments. First, the relation for $\mathbf{V}$ has resulted in no radial component in $\mathbf{u}_0^1$ to this order. Only the $e^{2i\varphi}$ forcing, added to the solid rotation, is of fundamental importance in the dynamics. Next, it is easily shown that $\mathbf{u}_0^1$ has zero azimuthal average. This means that the magnitude of the vorticity is 2 to this order, just the choice made earlier. Continuing, the boundary-layer singularity and the infinite efflux of this solution suggest some internal modification or deviation from solid rotation. Since such a deviation does not exist to any order in the linear theory, the next order in ϵ is the most likely path to show the interior modification. Formally, either the $\epsilon E^{\frac{1}{2}}$ or the $\epsilon^2 E^0$ orders may be considered next. The magnitudes of ϵ^2 and $\epsilon E^{\frac{1}{2}}$ are comparable in the earth, and can be made equal experimentally, so that taking the ϵ^2 order next is also valid physically.

3. The response for the second order in Rossby number

As was mentioned previously, the semidiurnal forcing frequency is the only important factor in determining $\mathbf{u}$. In fact, $\mathbf{u}_0^1$ had no radial component to the previous order. Hence, for simplicity, but without loss of generality, the shape of Σ can be taken as a sphere, and $\mathbf{V}$ will be presumed to now represent a stretching surface with a primarily $\cos 2\varphi$ variation.

$$\mathbf{V} = (1 + \tfrac{1}{2}\epsilon \cos 2\varphi)\hat{k} \times \mathbf{r}.$$

The results will only differ quantitatively by order e. This can be synthesized in the previous results by letting

$$q_0^1 \to 0, \quad e \to 0$$

but keeping ϵ fixed at the desired amplitude of excitation (thus invalidating (25)). This choice automatically has the surface stretching with the prescribed amplitude ϵ, and gives exactly the induced boundary-layer velocity just calculated, but with no $O(\epsilon)$ errors. Equation (19) is still an exact solution to the complete momentum equation, and is a geostrophic solution. The order $\epsilon^2 E^0$ momentum equation, for $e = 0$, is

$$(\mathbf{q}_0^2 . \nabla)\hat{k} \times \mathbf{r} + (\hat{k} \times \mathbf{r} . \nabla)\mathbf{q}_0^2 + (\mathbf{q}_0^1 . \nabla)\mathbf{q}_0^1 + \nabla p_0^2 = 0. \tag{28a}$$

Because $\mathbf{q}_0^1$ is zero, this is identical in form to (15). The continuity equation and the boundary condition are also similar, being

$$\nabla . \mathbf{q}_0^2 = 0, \quad \mathbf{q}_0^2 . \hat{n} = 0 \quad \text{on} \quad \Sigma, \tag{29), (30}$$

where, because of the modified geometry,

$$\hat{n} = \hat{r} \sin\theta + \hat{k} \cos\theta.$$

Equations (29) and (30) can be used to reduce the momentum equation to

$$2\hat{k}\times\mathbf{q}_0^2+\nabla p_0^2=0. \tag{28b}$$

A solution like (19) could be used for these equations, but it is not the most general choice. The general solution to (28*b*), (29), and (30) is

$$\mathbf{q}_0^2=\hat{k}\times\mathbf{r}f(|\hat{k}\times\mathbf{r}|), \tag{31}$$

with the function f being completely arbitrary. Thus, a deviation from constant vorticity is immediately suggested. The boundary-layer problem in the second order is given by

$$2\hat{k}\times\mathbf{u}_0^2-\hat{n}\frac{\partial\phi_1^2}{\partial\zeta}-\frac{\partial^2\mathbf{u}_0^2}{\partial\zeta^2}=-(\mathbf{u}_0^1.\nabla)\mathbf{u}_0^1+(\mathbf{u}_1^1+\mathbf{q}_1^1).\hat{n}\frac{\partial\mathbf{u}_0^1}{\partial\zeta}, \tag{32}$$

$$\frac{\partial}{\partial\zeta}(\mathbf{u}_1^2.\hat{n})+\hat{n}.\nabla\times(\hat{n}\times\mathbf{u}_0^2)-\hat{n}\times\mathbf{u}_0^2.\nabla\times\hat{n}=0, \tag{33}$$

$$\mathbf{q}_0^2+\mathbf{u}_0^2=0 \quad \text{on} \quad \Sigma. \tag{34}$$

First, carrying out the boundary condition to order $\epsilon E^{\frac{1}{2}}$, it is found that

$$(\mathbf{q}_1^1+\mathbf{u}_1^1).\hat{n}=0 \quad \text{on} \quad \Sigma. \tag{35}$$

Hence, the second inhomogeneous term on the right-hand side of (32) vanishes for an equatorial tide.

The arbitrary function f will be determined by the solvability condition for the interior equations of the order $\epsilon^2E^{\frac{1}{2}}$. Restricing them to just that part of the problem which is axisymmetric with respect to $\hat{k}$, they have the form

$$2\hat{k}\times\mathbf{q}_1^2+\nabla p_1^2=0, \tag{36}$$

$$\nabla.\mathbf{q}_1^2=0, \tag{37}$$

$$(\mathbf{q}_1^2+\mathbf{u}_1^2).\hat{n}=0 \quad \text{on} \quad \Sigma. \tag{38}$$

An immediate observation is that

$$(\hat{k}.\nabla)\mathbf{q}_1^2=0. \tag{39}$$

This is equivalent to the Taylor–Proudman theorem, but applies to the order $\epsilon^2E^{\frac{1}{2}}$ interior velocity. The consequence is that the part of the influx into the interior, which is symmetric with respect to the axis and the equatorial plane, has to vanish at any distance from the axis. This condition alone suffices to determine f, so it is necessary only to solve the axisymmetric part of the boundary-layer problem.

Since the non-axisymmetric part of the inhomogeneity in (32) is quadruply periodic about the axis, the corresponding part of (39) for the order $\epsilon^2E^{\frac{1}{2}}$ interior equations is generally fulfilled, which follows directly from the fact that no quadruply periodic solutions to the homogeneous part of the interior $\epsilon^2E^{\frac{1}{2}}$ problem can exist (Greenspan 1965, 1968).

Dividing the solution of (32) into two steps, the solution $\mathbf{u}_A$ of the homogeneous equation together with the inhomogeneous boundary condition is found first. Then, the solution $\mathbf{u}_B$ of the inhomogeneous equation with the boundary condition $\mathbf{u}_B=0$ on Σ is added. Since only the axisymmetric part of the problem

must be solved, the inhomogeneity in (32) is symmetric with respect to the equatorial plane. Hence, according to (39), the influx into the interior has to vanish.

$$\hat{n}\cdot\mathbf{u}_1^2|_{\zeta=0} = -\hat{n}\cdot\nabla\times\int_0^\infty \hat{n}\times\mathbf{u}_0^2 d\zeta + \hat{n}\times\int_0^\infty \mathbf{u}_0^2\cdot\nabla\times\hat{n}\,d\zeta = 0$$

$$= -\hat{n}\cdot\nabla\times\int_0^\infty \hat{n}\times\mathbf{u}_0^2 d\zeta.$$

Thus
$$\hat{n}\cdot\mathbf{u}_1^2|_{\zeta=0} = -\hat{n}\cdot\nabla\times\int_0^\infty \hat{n}\times(\mathbf{u}_A+\mathbf{u}_B)d\zeta = 0. \tag{40}$$

This will be sufficient to determine f. Then, by the same method used in §2, it is found that
$$(\hat{n}\times\mathbf{u}_A + i\mathbf{u}_A) = -[\hat{n}\times(\hat{k}\times\mathbf{r}) + i\hat{k}\times\mathbf{r}]f(r)e^{-\lambda\zeta}, \tag{41}$$
$$\lambda^2 = 2i\hat{k}\cdot\hat{n} = 2i\cos\theta,$$

such that

$$\mathbf{u}_A = -f(r)\{(\hat{n}\times(\hat{k}\times\mathbf{r}) + i\hat{k}\times\mathbf{r})e^{-\lambda\zeta} + (\hat{n}\times(\hat{k}\times\mathbf{r}) - i\hat{k}\times\mathbf{r})e^{-\lambda^*\zeta}\}. \tag{42}$$

The corresponding influx into the interior, from (40), is

$$-\hat{n}\cdot\nabla\times\int_0^\infty \hat{n}\times\mathbf{u}_A d\zeta = \frac{1}{\sqrt{(2\hat{k}\cdot\hat{n})}}\hat{n}\cdot\nabla\times\{[\hat{n}\times(\hat{k}\times\mathbf{r}) + i\hat{k}\times\mathbf{r}]f(r)\}. \tag{43}$$

The solution for $\mathbf{u}_B$ is a bit more lengthy. The equation is

$$\left(\frac{\partial^2}{\partial\zeta^2} - 2i\hat{k}\cdot\hat{n}\right)(\hat{n}\times\mathbf{u}_B + i\mathbf{u}_B) = [(-\hat{n}\times) + i\hat{n}\times(\hat{n}\times)](\mathbf{u}_0^1\cdot\nabla)\mathbf{u}_0^1.$$

Using (23) for $\mathbf{u}_0^1$, the inhomogeneous term can be written as follows (Busse 1968*a*):

$$[(-\hat{n}\times) + i\hat{n}\times(\hat{n}\times)](\mathbf{u}_0^1\cdot\nabla)\mathbf{u}_0^1 = -\tfrac{1}{4}\hat{k}\cdot\hat{n}[\hat{k}\times\mathbf{r} - i\hat{n}\times(\hat{k}\times\mathbf{r})]$$
$$\times\left\{\lambda e^{-(\lambda_+ + \lambda_-)\zeta} + \frac{i\zeta}{2\lambda_-}(1-\hat{k}\cdot\hat{n})e^{-(\lambda_+ + \lambda_-)\zeta}\right.$$
$$+\frac{i\zeta}{2\lambda_-}(1+\hat{k}\cdot\hat{n})e^{-(\lambda_- + \lambda_-^*)\zeta} + \frac{i\zeta}{2\lambda_+}(-1-\hat{k}\cdot\hat{n})e^{-(\lambda_+ + \lambda_-)\zeta}$$
$$\left.+\frac{i\zeta}{2\lambda_+}(1+\hat{k}\cdot\hat{n})e^{-(\lambda_+ + \lambda_+^*)\zeta}\right\}. \tag{44}$$

Now, using the boundary condition

$$\mathbf{u}_B = 0 \quad \text{on} \quad \Sigma$$

the solution is then that given below:

$$\hat{n}\times\mathbf{u}_B + i\mathbf{u}_B = -\tfrac{1}{4}[\hat{n}\times(\hat{k}\times\mathbf{r}) + i\hat{k}\times\mathbf{r}]\left\{\frac{e^{-(\lambda_+ + \lambda_-)\zeta} - e^{-\lambda\zeta}}{(\lambda_+ + \lambda_-)^2 - \lambda^2}\left[2i\hat{k}\cdot\hat{n}\right.\right.$$
$$\left.-\frac{(\lambda_+ + \lambda_-)}{(\lambda_+ + \lambda_-)^2 - \lambda^2}\frac{\hat{k}\cdot\hat{n}}{2}\left(\left\{\frac{1}{\lambda_-} - \frac{1}{\lambda_+}\right\} - \hat{k}\cdot\hat{n}\left\{\frac{1}{\lambda_-} + \frac{1}{\lambda_+}\right\}\right)\right]$$
$$-\frac{\zeta e^{-(\lambda_+ + \lambda_-)\zeta}}{(\lambda_+ + \lambda_-)^2 - \lambda^2}\frac{\hat{k}\cdot\hat{n}}{2}\left[\left(\frac{1}{\lambda_-} - \frac{1}{\lambda_+}\right) + \hat{k}\cdot\hat{n}\left(\frac{1}{\lambda_-} + \frac{1}{\lambda_+}\right)\right]$$

$$-\frac{\zeta e^{-(\lambda_-+\lambda_-^*)\zeta}}{(\lambda_-+\lambda_-^*)^2-\lambda^2}\frac{\hat{k}.\hat{n}}{2\lambda_-}(1+\hat{k}.\hat{n})$$

$$-\frac{\zeta e^{-(\lambda_++\lambda_+^*)\zeta}}{(\lambda_++\lambda_+^*)^2-\lambda^2}\frac{\hat{k}.\hat{n}}{2\lambda_+}(-1+\hat{k}.\hat{n})$$

$$-\frac{e^{-(\lambda_-+\lambda_-^*)\zeta}-e^{-\lambda\zeta}}{(\lambda_-+\lambda_-^*)^2-\lambda^2}\frac{\hat{k}.\hat{n}}{2\lambda_-}(1+\hat{k}.\hat{n})(\lambda_-+\lambda_-^*)$$

$$-\frac{e^{-(\lambda_++\lambda_+^*)\zeta}-e^{-\lambda\zeta}}{(\lambda_++\lambda_+^*)^2-\lambda^2}\frac{\hat{k}.\hat{n}}{2\lambda_+}(-1+\hat{k}.\hat{n})(\lambda_++\lambda_+^*)\Big\}. \tag{45}$$

Let
$$\hat{n}\times\mathbf{u}_B+i\mathbf{u}_B\equiv-\tfrac{1}{4}[\hat{n}\times(\hat{k}\times\mathbf{r})+i\hat{k}-\mathbf{r}]F_0, \tag{46}$$

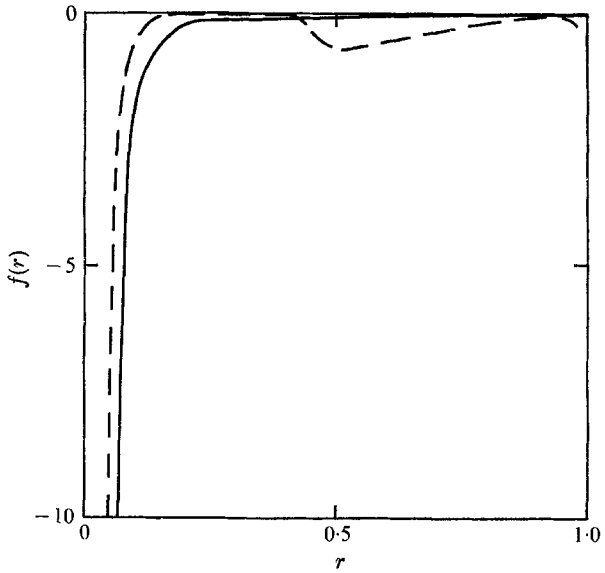

FIGURE 1. $f(r)$, the order e^2 angular velocity for tidally excited flow, *versus* radius. The theoretical result is plotted as a solid line, and the experimental result is plotted as a dashed line. The experimental parameters are: ω = 53 rev/min clockwise, streak interval = 60 revolutions, vertical container radius = 7·95 cm, e = 0·025.

and define
$$F\equiv\int_0^\infty F_0\,d\zeta. \tag{47}$$

Then, using these definitions, the influx corresponding to this solution is found as follows:

$$\hat{n}\times\mathbf{u}_B=-\tfrac{1}{8}\hat{n}\times(\hat{k}\times\mathbf{r})(F_0-F_0^*)-\tfrac{1}{8}i\hat{k}\times\mathbf{r}(F_0+F_0^*)$$

$$-\int_0^\infty\hat{n}.\nabla\times(\hat{n}\times\mathbf{u}_B)d\zeta=\tfrac{1}{8}\hat{n}.\nabla\times\{[\hat{n}\times(\hat{k}\times\mathbf{r})](F+F^*)\}$$

$$+\tfrac{1}{8}\hat{n}.\nabla\times\{i(\hat{k}\times\mathbf{r})(F-F^*)\}. \tag{48}$$

It is seen that only Im (F) need be investigated in detail, since the term proportional to $(F+F^*)$ is vanishing for any axisymmetric function F. The consequent result for $f(r)$ is

$$f(r)=-\tfrac{1}{4}i\sqrt{(|\hat{k}.\hat{n}|)}\frac{|\hat{k}.\hat{n}|}{\hat{k}.\hat{n}}(F-F^*). \tag{49}$$

This function, $f(r)$, represents the difference in angular velocities between the fluid and the container, divided by ϵ^2. It is plotted, as a solid line, in figure 1. The dotted line shows the experimental results, which will be discussed in the next section. $f(r)$ falls off as $1/r$ near the axis, and goes to zero as r approaches one.

These results can be directly combined with those of Busse, after taking into account the proper order of the shear. This is because there is no cross coupling between the two axially symmetric solutions, despite the non-linear character of the analysis. The combined results are discussed in terms of geophysical parameters by Suess (1969, 1970).

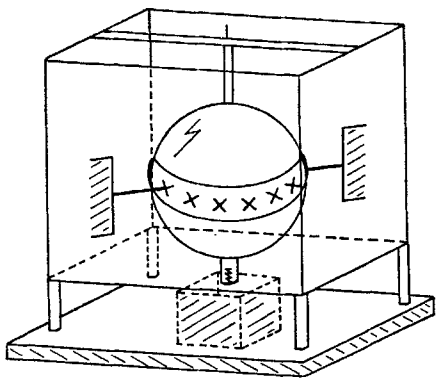

FIGURE 2. Schematic of the experimental apparatus; water tank, container, and deforming ring.

4. Laboratory experiment

In order to test the previous calculations, special apparatus was built. It consists of a clear, flexible water-filled ball, which is placed in a water-filled tank in order to isolate the ball from gravity. A shaft passes from the ball, through a water-tight seal, to a motor beneath the tank to provide for the rotation of the ball. The ball is deformed into an ellipsoid by a flat stainless-steel ring passing around its equator. The ring can be compressed along an axis through the equator, to give varying degress of ellipticity. In addition, the ring has perforations through which water may be pumped to form a friction decreasing water cushion between the ring and the ball. Along the long axis of the deformed ring, water may be sucked out, rather than pumped in, to force the ball to conform more nearly to the shape of the ring. A simplified sketch of the apparatus appears in figure 2.

The purpose of the experiment is to observe and confirm the theoretical results of the previous sections. However, since the ring can also be tilted through its short axis, the apparatus can be used to perform a much wider range of experiments. With a tilted ring, off-equator tides may be investigated, and the similarity of the flow to that in a precessing spheriod verified. The tiltover, and westward drift of the fluid resulting from the tiltover, may be measured and compared with previous theoretical and experimental work. Also, the stability of the flow to increasing tiltover, as well as to increasing equatorial

ellipticity, may be measured. A rotating table can be used to show the straightforward combination of precession and tidal driven flows. Finally, a rotating table can also be used to verify the width of the forced oscillation peak. This is done by placing the apparatus on the table, locating the ring on the equator, and rotating the table as the container is rotating. The fluid then sees a rotating ellipsoidal container, and is forced at a frequency either larger or smaller than 2ω, depending upon the sense of rotation of the table. These studies are still being carried out and will be reported on elsewhere. Here, the results for equatorial tides and laminar flow will be given and compared with the theory for any notable deviations. These results alone are a new and unique laboratory measurement of steady flows in a container, rotating fluid.

Measurements of the flow were made by inserting a dye streak across the interior of the container, at the equator, and measuring the dye trace as a function of time. Superposition of many streaks, individually produced at short intervals, allows fair resolution in the central region of the container, and very nicely shows the general features of the flow. The flow shown by the dye entirely disappears if e is adjusted to zero, ensuring that the source of the flow is truly the ellipticity of the equatorial streamline.

Two qualitative features are immediately illustrated by these dye streaks. First, the largest angular velocity in the rotating system is by far that at and near the axis of rotation. It is a retrograde shear zone orientated along the rotation axis and presents much the same aspect as that suggested by the solid line in figure 1. Also shown is a slower retrograde angular velocity peaking roughly at $r = \frac{1}{2}$. This is not present in the calculated values for $f(r)$, and so represents a measurable deviation from the theory. Because this feature is probably not simply a higher-order phenomenon in the set of equations, it must indicate a fundamental failing of the theory. It may be accounted for by interior viscosity effects not presently included in the interior equations.

Reducing the data to a form equivalent to $f(r)$, and plotting it alongside the computed $f(r)$, gives the results shown as a dotted line in figure 1. The experimental results have approximately the theoretical radial dimension of 0·1 radii, but do not approach the $1/r$ asymptotic value in $f(r)$ until significantly smaller values of r. The hump at $r = \frac{1}{2}$ now appears as a minor feature. However, the interaction producing this motion may be what leads to the suppression of the experimental profile, to almost exactly zero, down to a radius of about 0·1 radii. That the experimental profile does seem to approach $1/r$ eventually is very encouraging, indicating that viscosity effects are not completely dominant in this region.

The other quantitative aspect, which may be examined, is whether the amplitude of the vortex velocity depends on the square of the Rossby number. This is equivalent, in the experiment, to showing the dependence on e, the equatorial ellipticity. This comparison is shown in figure 3, with the data points plotted as circles. Also shown in this figure is the dependence of the flow at $r = \frac{1}{2}$, on e with the data points being plotted as triangles. First, it is noted that the best fit line through the circles has a slope of almost exactly $\frac{1}{2}$. This means that the angular velocity, at $r \gtrsim 0$, depends on the square of the ellipticity—as the

theory suggests. The line through the $r = \frac{1}{2}$ points is much steeper, indicating a very weak dependence on Rossby number. It may also be a curve, and in fact it may not even show a significant dependence on Rossby number.

It was mentioned, in §1, that precession driven flows also exhibit an axial vortex. The origin of this, in a spheroid, can be seen as follows. Precession causes the fluid vorticity vector to tilt away from the angular velocity vector of the container. When tilted, the streamlines become elliptical, due to the oblateness of the container, by an amount proportional to the oblateness and the tiltover angle. If η is the oblateness, and γ the tiltover, then the equivalent streamline ellipticity is $(\gamma\eta)$. Observations of the axial vortex in these precessing, rigid containers show that its amplitude does depend on $(\gamma\eta)^2$, lending additional experimental support to the theoretical results of §§2 and 3. These experimental results are from the work of Malkus which is, unfortunately, still unpublished.

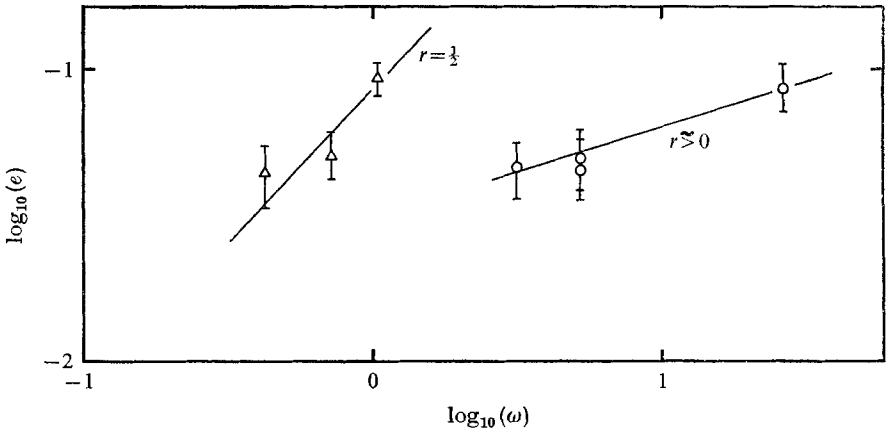

FIGURE 3. The fluid angular velocity, in the rotating system, for varying ellipticities. The values near $r = 0$ are plotted as circles, and those for $r = \frac{1}{2}$ are plotted as triangles. $\omega = 53$ rev/min, vertical container radius = 7·75 cm.

The quantitative accuracy of the results reported here is not too high, as indicated by the error bars in figure 3. However, it is sufficient to show, and confirm, the roll of the interaction of the semi-diurnal forcing with the inertial mode of the same frequency in producing an interior deviation from constant vorticity. The deviation is not precisely that predicted, the theoretical results being singular, but the amplitude dependence on Rossby number agrees well. The asymptotic approach of the angular velocity to $1/r$, for very small values of r, seems to be reached in the experiment. The actual flow, at $r = 0$, may deviate from $1/r$, but the experimental resolution of this region is very difficult.

The experiment can be refined, and used to study many other phenomena. Besides those cases mentioned earlier, there are many time-dependent flows attainable by using more general deformations of the container. In fact, the deformability of the container is perhaps the most interesting aspect of this experiment, offering many possibilities.

5. Discussion

Reviewing the calculations, they can be summarized as follows. First, the inviscid interior flow and the first-order boundary-layer correction were found. Next, instead of going to higher order in Ekman number to compensate for the first-order boundary-layer efflux, the second order in Rossby number effects was investigated. The second-order flow shows a retrograde vortex being formed along the rotation axis, whose vorticity amplitude increases as $1/r$ near the axis and is zero at $r = 1$. Finally, an experiment is described which verifies the main results of the theory, and suggests where and how the theory fails. All of these calculations are for laminar, non-stratified flow of low Ekman and Rossby numbers. The results are interesting enough to stand alone, on their own merit, in explaining the source and nature of a steady-state laboratory vortex. In addition, they can be used to make relevant hypotheses about the dynamics, and the source of waves and turbulence, in the core of the earth and in similar astrophysical situations.

It should be noted that the actual calculation for this second-order effect is somewhat simpler than that required by Busse. This is due to the absence of precession, and to the simpler geometry of having the boundary-layer singularities and the shear zone on the rotation axis. Thus, if a detailed analysis of the singular region were to be made, the surface could, to first order, be taken as horizontal. Busse (1968*b*) and Stewartson (1957, 1966) showed that having a sloping surface at the boundary-layer singularity and shear-layer intersection with the surface presented no fundamental theoretical restrictions, but did make the details of the analysis much more complex and obscure. They both resorted to planar geometries for their preliminary calculations. Consequently, the model discussed here offers a better choice for understanding and studying the basic nature of boundary-layer singularities, the excitation for free shear layers, and internal viscosity effects.

I wish to express my gratitude to Professor W. V. R. Malkus for suggesting this problem and for making many helpful suggestions towards its completion. During this work, aid was received from a NASA Predoctoral Traineeship, from NSF Grant GA-849, and is presently being received from an NRC-NAS Post-doctoral Research Associateship.

REFERENCES

Busse, F. 1968*a* *J. Fluid Mech.* **33**, 739.

Busse, F. 1968*b* *J. Fluid Mech.* **33**, 577.

Greenspan, H. 1965 *J. Fluid Mech.* **22**, 449.

Greenspan, H. 1968 *The Theory of Rotating Fluids.* Cambridge University Press.

Lamb, H. 1932 *Hydrodynamics.* Dover.

Stewartson, K. 1957 *J. Fluid Mech.* **3**, 17.

Stewartson, K. 1966 *J. Fluid Mech.* **26**, 131.

Stewartson, K. & Roberts, P. H. 1963 *J. Fluid Mech.* **17**, 1.

Suess, S. 1969 Doctoral dissertation, Department of Planetary and Space Science, U.C.L.A.

Suess, S. 1970 *J. Geophysical Res.* (in press).